

# Molecular Dynamics Simulations of Lipid Bilayers: Major Artifacts due to Truncating Electrostatic Interactions

M. Patra and M. Karttunen

*Biophysics and Statistical Mechanics Group, Laboratory of Computational Engineering,  
Helsinki University of Technology, P.O. Box 9203, FIN-02015 HUT, Finland*

M. T. Hyvönen

*Wihuri Research Institute, Kallioliinantie 4, FIN-00140 Helsinki,  
Finland, and Laboratory of Physics and Helsinki Institute of Physics,  
Helsinki University of Technology, P.O. Box 1100, FIN-02015 HUT, Finland*

E. Falck, P. Lindqvist, and I. Vattulainen

*Laboratory of Physics and Helsinki Institute of Physics,  
Helsinki University of Technology, P.O. Box 1100, FIN-02015 HUT, Finland*

(Dated: November 27, 2002)

We study the influence of truncating the electrostatic interactions in a fully hydrated pure dipalmitoylphosphatidylcholine (DPPC) bilayer through 20 ns molecular dynamics simulations. The computations in which the electrostatic interactions were truncated are compared to similar simulations using the Particle-Mesh Ewald (PME) technique. All examined truncation distances (1.8 to 2.5 nm) lead to major effects on the bilayer properties, such as enhanced order of acyl chains together with decreased areas per lipid. The results obtained using PME, on the other hand, are consistent with experiments. These artifacts are interpreted in terms of radial distribution functions  $g(r)$  of molecules and molecular groups in the bilayer plane. Pronounced maxima or minima in  $g(r)$  appear exactly at the cutoff distance indicating that the truncation gives rise to artificial ordering between the polar phosphatidyl and choline groups of the DPPC molecules. In systems described using PME, such artificial ordering is not present.

## I. INTRODUCTION

One of the great challenges in biophysics is to understand the basic principles that govern lipid bilayer mixtures. Lipid bilayers, or membranes, govern and mediate various biologically relevant processes on the cellular level. Transfer of ions through membranes and the function of enzymes attached to membranes provide two examples of these situations. Besides cellular membranes, lipid membranes are present in various man-made applications such as liposomes used in novel drug delivery techniques [1] and in many natural entities such as lipoproteins. The variety of situations where lipid bilayers play an important role is truly fascinating and is discussed in a number of review articles [2, 3, 4, 5, 6].

The characteristics of membranes have been extensively investigated for many decades, and experiments have provided substantial information about the intriguing physicochemical aspects of membrane systems [2, 3, 4, 5, 6]. However, while the experimental approach is the cornerstone of membrane research, it is often difficult or even impossible to obtain a thorough understanding of the phenomena taking place in lipid bilayers by experiments only. Therefore, atomistic computer simulation techniques such as classical molecular dynamics (MD) have become a standard tool for studies of biomembrane systems at the molecular level [4, 7, 8, 9].

One drawback of the computational approach is that its success depends on various methodological issues such as force fields, constraints, and the accuracy of integration schemes for the equations of motion [7, 10, 11, 12, 13]. In particular, the treatment of electrostatic interactions deserves special attention, since biomembrane systems are highly charged: lipid

molecules are either polar or charged and they interact with each other, the polar water environment, counterions [14], proteins [15], and DNA [16]. Proper treatment of electrostatic interactions in MD simulations is therefore one of the most important issues in this field and it continues to pose significant challenges for computer simulations.

The calculation of electrostatic interactions is typically based on solving the Poisson equation for the electrostatic potential such that all charged particles and their periodic images are taken into account in some systematic fashion. The Ewald summation method, its variants [17] and the fast multipole method [18, 19] are commonly used techniques that exploit this idea. In particular, the Particle-Mesh Ewald (PME) technique has been used increasingly often in lipid bilayer simulations [14, 20, 21, 22, 23].

Alternatively, one can neglect the long-range Coulombic tail and truncate the interactions at some suitable distance, a typical choice being 1.5–2.0 nm. This technique leads to considerable savings in the computational load and hence is widely used. Due to the speed-up, it is particularly useful in studies of large systems over long times [24, 25, 26], and when the computational requirements are demanding due to, e.g. long time scales associated with complex processes such as membrane fusion [27]. The discontinuities in the potential and forces at the cutoff radius are typically not considered to be a major issue, since they can be handled using various shifting and switching techniques [28, 29].

One might expect the artifacts due to truncation, if any, to become smaller as the cutoff distance  $r_{\text{cut}}$  is increased, and that for reasonably large cutoffs the system should not be influenced by truncation. In practice, however, this is

not the case. The classical example is water: its bulk properties [30, 31] and properties at the surfaces of lipid monolayers have been found to be affected by truncation [31, 32, 33]. Other cases where direct effects due to truncation have been observed include peptides, proteins, and DNA [15, 34, 35, 36, 37, 38].

Given these findings, it is rather surprising that only Venable et al. have considered the effects of truncation in the context of lipid bilayers [20]. They compared the areas per molecule in a DPPC bilayer in the gel phase using systems in which the electrostatic interactions had been treated using PME and a truncation of 1.2 nm. They found the results to differ by about 4 %. To the best of our knowledge, further systematic studies of truncation effects in lipid bilayers have not been reported. The lack of information is particularly striking in the case of the liquid-crystalline ( $L_\alpha$ ) phase, which is highly relevant from a physiological point of view. Instead, the general impression seems to be that truncation may lead to artifacts, but they are minor, or even negligible, if the cutoff is longer than about 1.8 nm [31, 32, 33, 39].

In this article, we show through an extensive set of 20 ns MD simulations for a fully hydrated pure lipid bilayer of 128 dipalmitoylphosphatidylcholine (DPPC) molecules in the liquid-crystalline phase that the truncation of electrostatic interactions can have significant consequences on the properties of lipid bilayer systems. We consider several truncation distances from 1.8 to 2.5 nm and compare them to a case where the Particle-Mesh Ewald technique has been applied. We find that the simulations where PME has been used lead to an area per lipid molecule consistent with experiments, while the truncation of electrostatic interactions leads to 5–14 % smaller values. This dramatic result is reflected in various properties of the lipid bilayer, including the probability distribution of the area per lipid, the density profile across the membrane, and the ordering of acyl chains. In addition to these, truncation leads to prominent artifacts in the electrostatic potential across the bilayer. We interpret the artifacts in terms of radial distribution functions  $g(r)$  of molecules and molecular groups in the plane of the membrane. The radial distribution functions reveal without doubt that truncation leads to artificial ordering in the head groups of lipid molecules.

We conclude that the truncation of electrostatic interactions may lead to profound artifacts in the properties of lipid bilayer systems, and should be used with great care, if at all.

## II. SYSTEM

### A. Model and simulation details

We have simulated a lipid bilayer system consisting of 128 DPPC molecules (shown schematically in Fig. 1), fully hydrated by 3655 water molecules. The united atom model description used in this work has been validated previously [40].

We used a system available at <http://moose.bio.ucalgary.ca/files/dppc128.pdb> as our initial configuration. This system corresponds to the final structure of run E discussed elsewhere [40]. The bilayer is in the  $x$ - $y$

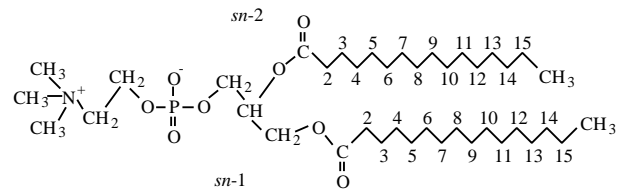


FIG. 1: Representation of a DPPC molecule showing the numbering of carbons in the acyl chains discussed in the text.

plane.

The parameters for bonded and non-bonded interactions were taken from a rather recent study on a DPPC bilayer system [41], available in electronic form at <http://moose.bio.ucalgary.ca/files/lipid.itp>. The partial charges were obtained from the underlying model description [40] and can be found at <http://moose.bio.ucalgary.ca/files/dppc.itp>. For water, the SPC model [42] was used.

Lennard-Jones interactions were cut off at 1.0 nm without shift or switch functions. Electrostatic interactions within 1.0 nm were calculated at each time step, while interactions beyond this range were determined every ten timesteps. These choices follow the parameterization of DPPC [40]. Long-range electrostatics was handled either by using a cutoff at  $r_{\text{cut}} = 1.8$  nm, 2.0 nm, or 2.5 nm, or by means of the Particle-Mesh Ewald [43] method to take the long-range interaction fully into account. The time step for the simulations was chosen to be 2.0 fs.

The simulations were performed using the Gromacs [44] package in the  $NpT$  ensemble. The Berendsen algorithm with a time constant of 1 ps for pressure coupling was used as barostat. The setup was chosen such that the height of the simulation box (i.e., its extension in the  $z$ -direction) was allowed to vary independently of the cross-sectional area of the box in the  $x$ - $y$  plane. The DPPC and water molecules were separately coupled to a heat bath at a temperature  $T = 323$  K using the Berendsen algorithm [45] with a coupling constant of 0.1 ps. The lengths of all bonds were kept constant with the Lincs algorithm [46].

The main focus of this paper is on the effects due to different treatments of the long-range electrostatic interactions. To this end, we have studied DPPC bilayers over a time scale of 20 ns using three different truncation distances and PME. The simulations have been repeated at two different temperatures in the liquid-crystalline phase to confirm the validity of our conclusions. In addition, as described in Appendix A, we performed additional simulations to examine the effects due to constraints, time constants of the thermostat and pressure coupling, and the range of van der Waals interactions. These simulations sum up to about 20 simulations of 20 ns each. In total, the simulations took about 15 000 CPU hours.

## B. Data analysis

To calculate the area occupied by each individual lipid and to determine the probability distributions for the area per lipid  $P(A)$ , we applied Voronoi analysis in two dimensions [47]. In Voronoi tessellation, we first computed the centers of mass (CM) for the lipids and projected them onto the  $x$ - $y$  plane. Thus, the centers of mass define a set of points in the  $x$ - $y$  plane. A point in the plane is considered to belong to a particular Voronoi cell if it is closer to the projected CM of the lipid molecule associated with that cell than to any other CM position.

The mass density profile across the bilayer was calculated by separately analyzing each frame of the simulations. The center of the bilayer (i.e., its  $z$ -component) was first determined by computing the centers of mass for the two monolayers. The positions of all atoms were then taken into account with respect to the center. It is important to note that the masses of all hydrogen atoms must be included explicitly, as has been done in this work. Since the system possesses mirror symmetry, all positions with  $z < 0$  have been folded to  $z > 0$  to reduce statistical error.

The electrostatic potential across the bilayer was calculated in a similar fashion. The average charge density profile was first computed in such a way that the center of the bilayer ( $z = 0$ ) was determined for each simulation frame separately. Finally, the electrostatic potential was determined by integrating the charge density twice starting from the initial condition  $V(z = 0) = 0$ .

The microscopic structure of lipid molecules and the ordering of acyl chains is characterized through the order parameter tensor  $S_{\alpha\beta}$  ( $\alpha, \beta = x, y, z$ ) defined as

$$S_{\alpha\beta} = \frac{1}{2} \langle 3 \cos \theta_\alpha \cos \theta_\beta - \delta_{\alpha\beta} \rangle, \quad (1)$$

where  $\theta_\alpha$  is the angle between the  $\alpha^{\text{th}}$  molecular axis and the bilayer normal ( $z$ -axis). The order parameter is calculated separately for all positions (carbons) along the chain. Given the geometry of the bilayer, the relevant order parameter is the diagonal element  $S_{zz}$ . This is related to the deuterium order parameter  $S_{\text{CD}}$  defined as

$$S_{\text{CD}} = \frac{2}{3} S_{xx} + \frac{1}{3} S_{yy}, \quad (2)$$

which is often determined in experiments, e.g. using nuclear magnetic resonance spectroscopy. Since the bilayer is symmetric with respect to rotation around the  $z$ -axis, we have  $S_{xx} = S_{yy}$ , and  $S_{xx} + S_{yy} + S_{zz} = 0$ . Hence, it follows that  $S_{\text{CD}} = -S_{zz}/2$ . To allow comparison with experimental data, we present our results in terms of  $|S_{\text{CD}}|$ .

Ordering of water in the vicinity of the bilayer-water interface is described by calculating the time averaged projection of the water dipole unit vector  $\vec{\mu}(z)$  onto the interfacial normal  $\vec{n}$ ,

$$P(z) = \langle \vec{\mu}(z) \cdot \vec{n} \rangle = \langle \cos \theta \rangle, \quad (3)$$

where  $z$  is the  $z$ -component of the center of mass of the water molecule and vector  $\vec{n}$  points away from the bilayer center along the  $z$ -coordinate.

In order to calculate the radial distribution functions (RDFs) between different charged groups, one should note that the groups have internal structure. The positively charged group is choline, essentially  $\text{N}(\text{CH}_3)_3^+$ , and the negatively charged one is the phosphate group, essentially  $\text{PO}_2\text{O}^-$ . To demonstrate possible artifacts due to truncation in the pair correlation behavior between these charged groups, we found that the most transparent way to this end is to consider RDFs between nitrogen and phosphate atoms in the choline and phosphate groups. The RDFs presented in this work are thus for the P–P and N–N pairs.

Note that our simulations—like virtually all simulations—use a group based cutoff, i.e., electrostatic interactions are computed for a pair of particles if any pair belonging to the two groups is within the cutoff distance. Due to this, the system cannot force any atom to a certain distance such that it would artificially enhance favorable interactions within a group only. As a consequence, the artifacts observed using truncated electrostatics cannot be explained by the internal structure.

For the radial distribution function between the center of mass positions of the DPPC molecules, we first calculated the CM for all of them. Then, the  $g_{2d}(r)$  was computed in a plane, i.e., using the  $x, y$ -coordinates of the CM positions.

## III. RESULTS AND DISCUSSION

### A. System dimensions

One of the central quantities in describing lipid bilayers is the average area per molecule  $\langle A \rangle$ . For DPPC it has been experimentally determined to be  $\langle A \rangle = 0.64 \text{ nm}^2$  [5]. It provides a measure for tuning the force fields and other parameters for lipid systems as one aims for a quantitative description of lipid bilayers through MD simulations. In the present work, the average area per lipid was computed using the size of the simulation box in the  $x$ - $y$  plane. Since we employ pressure coupling, the simulation box is allowed to fluctuate during the simulation. The temporal behavior of the area per lipid  $A(t)$  is shown in Fig. 2. The simulations have equilibrated after 10 ns and for the analysis we discarded the first 10 ns, and used the second 10 ns period only.

Fig. 2 shows that  $A(t)$  depends strongly on the treatment of electrostatic interactions. The simulations using PME yielded  $\langle A \rangle = (0.645 \pm 0.010) \text{ nm}^2$  consistent with recent experiments [5]. Truncation at both 2.0 nm and 2.5 nm lead to  $\langle A \rangle = (0.615 \pm 0.010) \text{ nm}^2$ , which deviates about 5% from the PME result. Further decrease of the cutoff distance to 1.8 nm lead to  $\langle A \rangle = (0.555 \pm 0.010) \text{ nm}^2$ . This is about 14% smaller than the reference value of  $0.645 \text{ nm}^2$ .

We verified that the large differences in the average area per lipid are indeed due to electrostatics and not a consequence of initial conditions. To this end, we chose an equilibrated configuration from the simulation with  $r_{\text{cut}} = 1.8 \text{ nm}$  (at 10 ns) as the initial configuration for a new simulation. In this new simulation, the electrostatic interactions were computed using PME instead of a cutoff. This transition point is marked by an

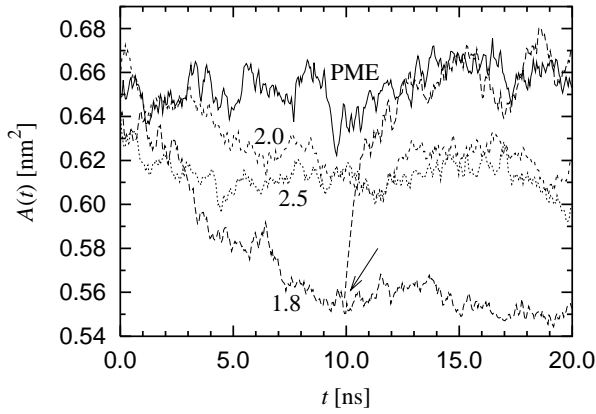


FIG. 2: The area per lipid  $A(t)$  as a function of time for truncated and PME electrostatics. Cutoff radii are shown in the plot. In addition,  $A(t)$  is shown for the case where the electrostatics was switched from a cutoff at 1.8 nm to PME at 10 ns (marked by an arrow).

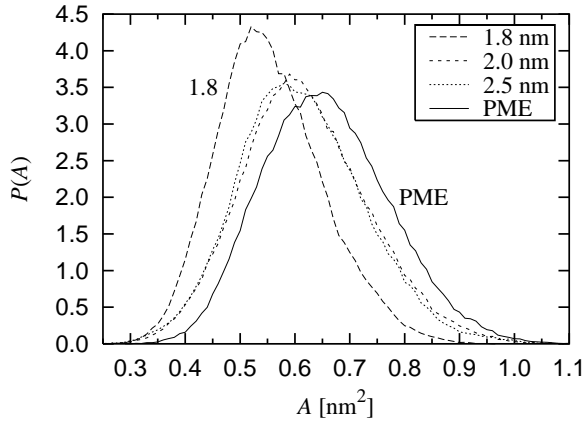


FIG. 3: Distribution of the area per lipid,  $P(A)$ , computed by the Voronoi analysis.

arrow in Fig. 2. As seen from Fig. 2, the area per lipid quickly approaches the value of  $0.645 \text{ nm}^2$ . We can thus conclude that the different areas per lipid reported here are solely due to the treatment of electrostatic interactions.

For the purpose of comparison, let us note that our results for the average area per lipid at short times are in agreement with earlier studies by Tieleman et al. [40], whose model description we follow in the present work. They used a cutoff at 2.0 nm and found  $\langle A \rangle \approx 0.60 \text{ nm}^2$  for the area per molecule. A full comparison is not meaningful, however, since the time scale in their studies was 0.5 ns and the analysis was done over the last 100 ps only.

We have extended the above studies by considering the probability distributions for the area per lipid molecule  $P(A)$ . This quantity is of interest for a number of processes in lipid bilayers, e.g. the lateral diffusion of lipids in the bilayer plane. Results for  $P(A)$  are shown in Fig. 3. The distributions reveal

that the minimum area per lipid is approximately  $0.3 \text{ nm}^2$ . Further, we find that the shapes of the distributions are similar and scaled by the average area per molecule. However, it is worth pointing out that even if the cutoff distance is increased to a value close to the maximal one (i.e., half of the linear dimension of the system), the artifacts in  $P(A)$  persist. This indicates that cutoff distances even as large as 2.5 nm are not sufficient for a proper quantitative treatment of electrostatics.

Next we estimate the density distribution and the dimensions along the bilayer normal. The mass density profile for water and lipid molecules is shown in Fig. 4. As before, we find that the smallest cutoff leads to major artifacts as compared to the PME description, while the other two truncation distances perform better. The results obtained using any truncation distance are distinctly different from those obtained using PME, however. To demonstrate this, we consider the thickness of the bilayer defined as the point where the densities of water and lipids are equal. The half-thicknesses of the bilayers were found to be 2.03 nm for PME, 2.15 nm for  $r_{\text{cut}} = 2.0 \text{ nm}$  and 2.5 nm, and 2.33 nm for  $r_{\text{cut}} = 1.8 \text{ nm}$ . It is noteworthy that the deviations in these results are of similar size as the deviations found in the average area per molecule. However, while truncation leads to a *decreased* area per lipid, it also leads to an *increased* height of the membrane. Thus these two artifacts compensate each other, and one finds that the average volume per lipid obtained by truncation methods is consistent with the value found by PME. This result was confirmed by the Voronoi analysis for the lipid bilayers in three dimensions (data not shown).

It should be noted that the density of the bulk water phase is essentially independent of the simulation parameters. This is in contrast to the density of the lipid phase. These observations confirm that the differences between the simulations are caused by the electrostatic interactions between the lipids and/or lipids and water, but not by the interactions among the water molecules.

## B. Order parameters

We have computed  $S_{\text{CD}}$  for all carbon atoms in both chains (*sn*-1 and *sn*-2) by averaging over all equivalent atoms in all DPPC molecules. The results are shown in Fig. 5. We find that PME yields an order parameter profile which is in good agreement with experimental data [48, 49, 50]. Note that  $S_{\text{CD}} \approx 0.20$  close to the glycerol group, and tends towards zero toward the end of a tail. The acyl chains are therefore reasonably ordered close to the head group, while conformational disorder becomes more and more apparent towards the center of the bilayer.

The results with different cutoff distances differ significantly from those obtained using PME. The situation close to the glycerol group clearly demonstrates the problem. The truncation of electrostatic forces at  $r_{\text{cut}} = 2.0 \text{ nm}$  and 2.5 nm yields order parameters that deviate about 13% from the values obtained using PME. In the case of  $r_{\text{cut}} = 1.8 \text{ nm}$ , the deviation is even larger, being of the order of 40% close to

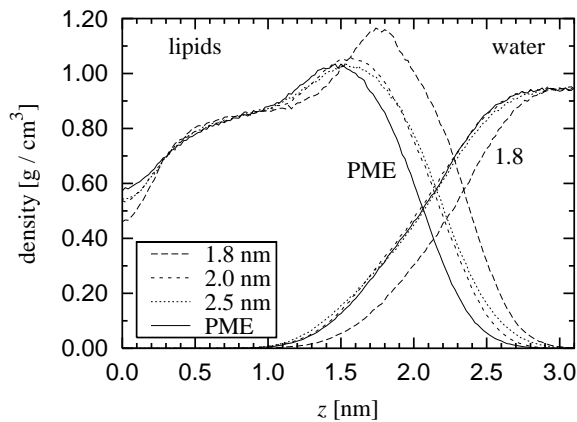


FIG. 4: Mass density profile across the bilayer computed separately for lipids (left) and water (right).  $z = 0$  corresponds to the center of the bilayer and both sides of the bilayer have been folded towards positive  $z$ .

the glycerol group. Differences are expected since the ordering of acyl chains must be affected by the packing of lipids as discussed in the previous section. A reduction in the area per molecule leads to an enhanced ordering of the acyl chains and correlates with an increased thickness of the bilayer.

We have also considered the ordering of water in the vicinity of the bilayer-water interface by calculating the time averaged projection of the water dipole unit vector onto the interfacial normal. As revealed by Fig. 6, the water molecules prefer to order themselves in such a way that the dipoles are oriented towards the bilayer. Ordering persists up to the height where the density of the lipids approaches zero.

This ordering can be explained by the orientational behavior of water molecules around phosphoryl groups. The radial distribution of the oxygens and hydrogens of the water molecules around the phosphatidyl and choline groups were determined (data not shown), revealing that the water molecules are strongly oriented around the phosphorus atom. This is due to the hydrogen bonding between the oxygen atoms of the phosphatidyl group and the hydrogen atoms of the water molecules. Only a weak orientation is found around the nitrogen atom, most likely due to the hydrophobic nature of the surrounding methyl groups, which results in hydrogen bonding among the water molecules. This behavior is very similar for the different treatments of electrostatic interactions and also to earlier MD simulation studies of phosphatidylcholine systems [32, 51, 52, 53]. As the number of hydrogen-bonded water molecules around the phosphatidyl group is larger on the side of the water region, the dominating orientation of the water dipoles is toward the bilayer center. Only a few water molecules penetrate into the hydrocarbon region, resulting in poor statistics and a spiky profile.

To conclude this section, our results indicate that the ordering of fatty acyl chains is strongly affected by the method by which electrostatic interactions are treated. In addition, we find that the use of a relatively large cutoff in electrostatic

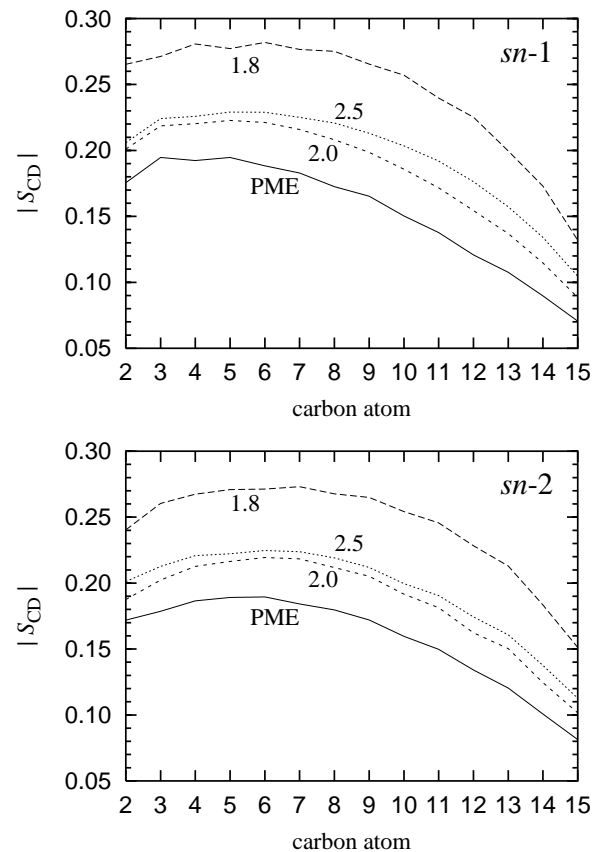


FIG. 5: The order parameter  $|S_{CD}|$  separately for the two acyl chains of DPPC: *sn*-1 chain and *sn*-2 chain. For numbering of carbons, see Fig. 1.

interactions does not give rise to major artifacts in the properties of water molecules themselves or their radial distribution around the head groups. At the surface of the bilayer, however, packing of lipids affects the properties of the interfacial water layer. These conclusions support the view of previous research on the properties of water close to a water-lipid monolayer interface [31, 32, 33]. In these studies it was found that the artifacts were reduced by an increase in the cutoff, but were not eliminated for cutoff distances as large as  $r_{\text{cut}} = 1.8$  nm. The work by Feller et al. provides a particularly interesting example of this issue, since they considered the radial distribution of oxygen-oxygen pairs in bulk water and found minor peaks close to the cutoff distance [31]. This is consistent with our results for RDFs close to the water-bilayer interface. We studied the radial distribution functions for O-N and O-P pairs (where O stands for oxygen in water) and found very weak but systematic ordering effects at  $r_{\text{cut}}$ . In RDFs found by PME, such ordering effects were not present.

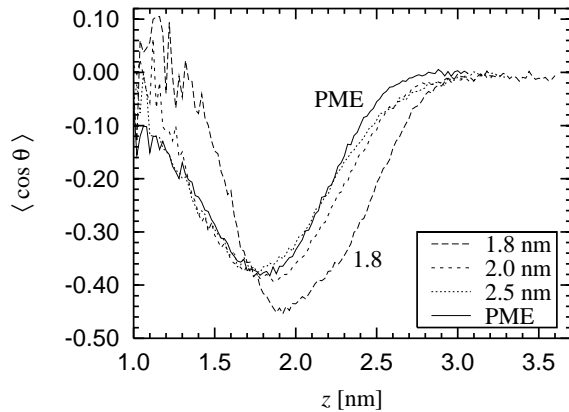


FIG. 6:  $P(z) = \langle \cos \theta \rangle$  describing the ordering of water close to the bilayer-water interface.  $z = 0$  corresponds to the center of the bilayer. The noise at small  $z$  is due to the small number of water molecules inside the bilayer.

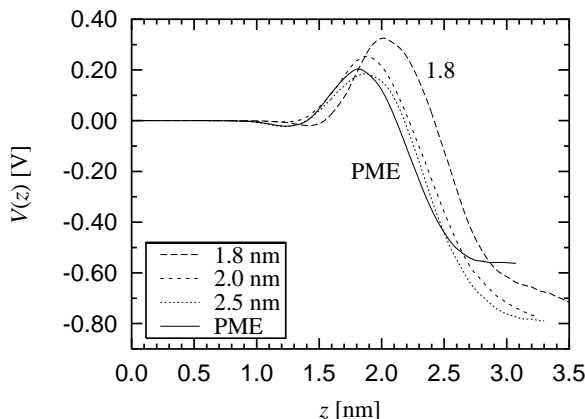


FIG. 7: Total electrostatic potential  $V(z)$  across the bilayer, where  $z = 0$  corresponds to the center of the bilayer.

### C. Electrostatic potential

Based on the results discussed above, it seems obvious that the truncation of Coulombic interactions plays an important role in the electrostatic properties of the bilayer. To verify this and to quantify the magnitude of possible artifacts due to truncation, we studied the electrostatic potential  $V(z)$ . The results are shown in Fig. 7.

The general behavior agrees with previous simulation studies of PC bilayers [40, 54, 55, 56]. The lipid molecules contribute with a large positive potential, which is compensated by the contribution due to the water molecules. The total potential was determined to be  $-570$  mV. For comparison, the experimental values for the potential range from  $-200$  mV to  $-575$  mV for different PC/water interfaces [57, 58, 59, 60].

As what comes to the differences between the curves in Fig. 7, we note that the profiles of  $V(z)$  are correlated with the mass density profiles in Fig. 4. The differences in the packing

of lipids are also reflected in the electrostatic potential: The strongest orientation of water molecules is found just above the peak in the density of lipids, and the orientation of the water ranges just as far as the head groups of the lipids prevail.

### D. Radial distribution of lipids

We first consider RDFs between the two charged groups in a DPPC molecule. The positively charged choline group is at the top and the negatively charged phosphate group at the lower part of the head group (see Fig. 1). However, the average orientation of the P–N vector is almost parallel to the plane of the bilayer (data not shown). The details of the calculation are described in Sec. II B.

The RDFs for the two pairs of P and N atoms in the head group are shown in Fig. 8. The RDF of N–N pairs serves as a good example of our findings. The application of PME yields a radial distribution function which has a hard core at small distances, a rather narrow peak around  $0.8$  nm, and essentially no structure beyond  $r = 1.0$  nm. This behavior is expected since we are dealing with a liquid-crystalline phase in the absence of translational order in the bilayer plane. The RDFs from the simulations in which a cutoff was used are dramatically different. In all of these cases we find that there is a wildly oscillating long-range component which has a local maximum exactly at the cutoff distance. In addition to this, the oscillations persist for distances far beyond  $r_{\text{cut}}$ . Although the details are slightly different for P–P (as well as N–P) pairs, similar conclusions on artificial ordering can be drawn.

These structural artifacts have a very strong character. This is evident from the RDF for the DPPC center of mass positions presented in Fig. 9. The  $g(r)$  given by the PME method is consistent with the assumption of a fluid-like phase, having just a small peak around  $1.2$  nm. The truncation methods, on the other hand, give rise to further structure manifested as artificial maxima precisely at the cutoff distance.

Results of similar nature have been reported for ionic systems [10]. For an aqueous NaCl solution van Gunsteren and Mark found that the truncation of Coulombic interactions gave rise to an artificial peak around the cutoff distance. In our work the DPPC molecules are polar, though the behavior of the bilayer is not expected to be solely dictated by polar groups. In this sense, the pronounced artifacts in Fig. 9 for lipid molecules may come as a surprise.

We can conclude that the truncation of electrostatic interactions gives rise to artificial order in the plane of the membrane. Truncation changes the phase behavior of the bilayers, and consequently affects thermodynamic properties such as the compressibility of the bilayer. It is clear that this is a matter of serious concern. It suggests that the truncation of Coulombic interactions in lipid bilayer systems may not only influence the short-range order of the system, but also the long-range behavior. Various intriguing phenomena such as organization of bilayer-protein systems involve scales of several molecular diameters. The artificial ordering observed in this work persists over these distances, and care should be taken when treating these systems.

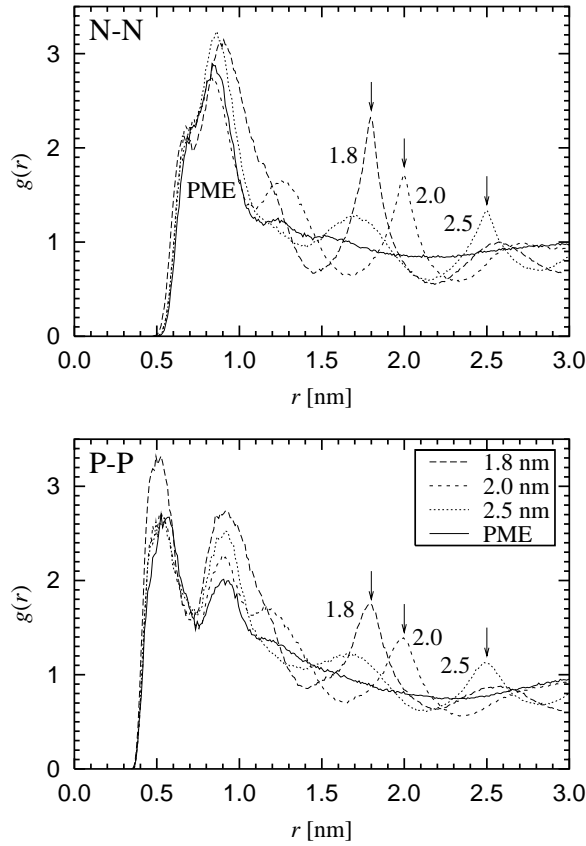


FIG. 8: Radial distribution function (RDF)  $g(r)$  between the two central atoms in the headgroup of a DPPC molecule: RDFs for N–N and P–P pairs. Cutoff distances are indicated by arrows.

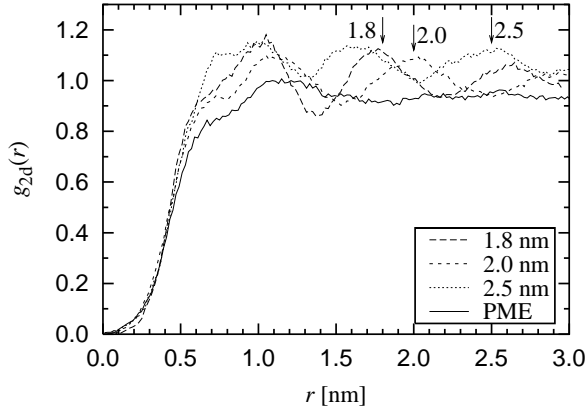


FIG. 9: Radial distribution function  $g_{2d}(r)$  for the center of mass positions of the DPPC molecules. Note the relatively soft core of  $g(r)$  in the vicinity of  $r = 0$ . This is due to the fact that the lipids may be entangled around each other such that the  $x, y$ -coordinates of their center of mass positions may lie close to each other.

#### IV. SUMMARY AND CONCLUSIONS

We have investigated the effects of truncating Coulombic interactions on the properties of a DPPC bilayer and water in the vicinity of a bilayer-water interface. We have found that the truncation of electrostatic interactions can have serious consequences for the structural and electrostatic properties of lipid bilayer systems. The reduced area per molecule and the corresponding changes in the ordering of acyl chains provide two examples of the problems associated with truncation. As shown in this work, these artifacts are due to the fact that truncation gives rise to artificial ordering in the bilayer plane, which in turn implies that the lipid bilayer is no longer in a truly fluid-like state. Instead, the artificial order persists over a long range, which for typical system sizes studied by molecular dynamics simulations may exceed the actual size of the system. Furthermore, since the artificial order due to truncation affects the phase behavior of the system, we may conclude that there is indeed a reason for major concern.

The Particle-Mesh Ewald (PME) technique, on the other hand, has performed very well in this study. Besides providing results consistent with experimental data, it has given no reason for concern with respect to pair correlation behavior in the plane of the bilayer. The current trend of using PME in MD simulations of lipid membrane systems seems to be justified and should be encouraged.

We would like to stress, however, that even PME and its variants may lead to artifacts unless great care is taken. These artifacts are related to the periodicity of the system, as periodic boundary conditions are used to eliminate finite size effects in simulations of small systems. Hünenberger et al. have observed [61, 62] that the artificial periodicity used in Ewald techniques may indeed affect the conformational equilibria of e.g. peptides and proteins by stabilizing the most compact conformations of the molecules. It is clear that more attention is called for to develop more reliable and efficient techniques for dealing with electrostatic interactions in simulations of biomolecular systems.

*Acknowledgements* — This work has, in part, been supported by the Academy of Finland through its Center of Excellence Program (E.F., P.L., and I.V.), the National Graduate School in Materials Physics (E.F.), the Academy of Finland Grant No. 54113 (M.K.), the Jenny and Antti Wihuri Foundation (M.H.) and the Federation of Finnish Insurance Companies (M.H.).

- 24**, 293 (1991).
- [3] R. Lipowsky and E. Sackmann, eds., *Structure and dynamics of membranes: From cells to vesicles* (Elsevier, Amsterdam, 1995).
  - [4] K. M. Merz, Jr. and B. Roux, eds., *Biological membranes: A molecular perspective from computation and experiment* (Birkhäuser, Boston, 1996).
  - [5] J. F. Nagle and S. Tristram-Nagle, *Biochim. Biophys. Acta*. **1469**, 159 (2000).
  - [6] J. Katsaras and T. Gutberlet, eds., *Lipid bilayers: Structure and interactions* (Springer-Verlag, Berlin, 2001).
  - [7] D. P. Tieleman, S. J. Marrink, and H. J. C. Berendsen, *Biochim. Biophys. Acta*. **1331**, 235 (1997).
  - [8] S. E. Feller, *Curr. Opin. Colloid Interface Sci.* **5**, 217 (2000).
  - [9] L. Saiz and M. L. Klein, *Acc. Chem. Res.* **35**, 482 (2002).
  - [10] W. F. van Gunsteren and A. E. Mark, *J. Chem. Phys.* **108**, 6109 (1998).
  - [11] S.-W. Chiu, M. Clark, S. Subramaniam, and E. Jacobsson, *J. Comput. Chem.* **21**, 121 (2000).
  - [12] G. Besold, I. Vattulainen, M. Karttunen, and J. M. Polson, *Phys. Rev. E*. **62**, R7611 (2000).
  - [13] I. Vattulainen, M. Karttunen, G. Besold, and J. M. Polson, *J. Chem. Phys.* **116**, 3967 (2002).
  - [14] S. A. Pandit and M. L. Berkowitz, *Biophys. J.* **82**, 1818 (2002).
  - [15] G. T. Ibragimova and R. C. Wade, *Biophys. J.* **74**, 2906 (1998).
  - [16] S. Bandyopadhyay, M. Tarek, and M. L. Klein, *J. Phys. Chem. B*. **103**, 10075 (1999).
  - [17] C. Sagui and T. A. Darden, *Annu. Rev. Biophys. Biomol. Struct.* **28**, 155 (1999).
  - [18] L. Greengard and V. Rokhlin, *J. Comp. Phys.* **73**, 325 (1987).
  - [19] D. Frenkel and B. Smit, *Understanding molecular simulation: From algorithms to applications, 2nd edition* (Academic Press, San Diego, 2002).
  - [20] R. M. Venable, B. R. Brooks, and R. W. Pastor, *J. Chem. Phys.* **112**, 4822 (2000).
  - [21] L. Saiz and M. L. Klein, *Biophys. J.* **81**, 204 (2001).
  - [22] S. E. Feller, K. Gawrisch, and A. D. MacKerell, Jr., *J. Am. Chem. Soc.* **124**, 318 (2001).
  - [23] D. J. Tobias, *Curr. Opin. Struct. Biol.* **11**, 253 (2001).
  - [24] E. Lindahl and O. Edholm, *Biophys. J.* **79**, 426 (2000).
  - [25] S. J. Marrink, E. Lindahl, O. Edholm, and A. E. Mark, *J. Am. Chem. Soc.* **123**, 8638 (2001).
  - [26] S. W. Chiu, E. Jacobsson, R. J. Mashl, and H. L. Scott, *Biophys. J.* **83**, 1842 (2002).
  - [27] S. J. Marrink and D. P. Tieleman, *Biophys. J.* **83**, 2386 (2002).
  - [28] P. J. Steinbach and B. R. Brooks, *J. Comput. Chem.* **15**, 667 (1994).
  - [29] A. R. Leach, *Molecular modelling: Principles and applications, 2nd edition* (Prentice Hall, Harlow, 2001).
  - [30] H. E. Alper and R. M. Levy, *J. Chem. Phys.* **91**, 1242 (1989).
  - [31] S. E. Feller, R. W. Pastor, A. Rojnuckarin, S. Bogusz, and B. R. Brooks, *J. Phys. Chem.* **100**, 17011 (1996).
  - [32] H. E. Alper, D. Bassolino, and T. R. Stouch, *J. Chem. Phys.* **98**, 9798 (1993a).
  - [33] H. E. Alper, D. Bassolino-Klimas, and T. R. Stouch, *J. Chem. Phys.* **99**, 5547 (1993b).
  - [34] P. E. Smith and B. M. Pettitt, *J. Chem. Phys.* **95**, 8430 (1991).
  - [35] H. Schreiber and O. Steinhauser, *Biochemistry*. **31**, 5856 (1992).
  - [36] D. M. York, T. A. Darden, and L. G. Pedersen, *J. Chem. Phys.* **99**, 8345 (1993).
  - [37] D. M. York, W. Yang, H. Lee, T. Darden, and L. G. Pedersen, *J. Am. Chem. Soc.* **117**, 5001 (1995).
  - [38] J. Norberg and L. Nilsson, *Biophys. J.* **79**, 1537 (2000).
  - [39] E. Jakobsson, S. Subramaniam, and H. L. Scott, in *Biological membranes – A molecular perspective from computation and experiment*, edited by K. M. Merz, Jr. and B. Roux (Birkhäuser, Boston, 1996), chap. 4, pp. 105–123.
  - [40] D. P. Tieleman and H. J. C. Berendsen, *J. Chem. Phys.* **105**, 4871 (1996).
  - [41] O. Berger, O. Edholm, and F. Jahnig, *Biophys. J.* **72**, 2002 (1997).
  - [42] H. J. C. Berendsen, J. P. M. Postma, W. F. van Gunsteren, and J. Hermans, in *Intermolecular Forces*, edited by B. Pullman (Reidel, Dordrecht, 1981), pp. 331–342.
  - [43] U. Essman, L. Perera, M. L. Berkowitz, H. L. T. Darden, and L. G. Pedersen, *J. Chem. Phys.* **103**, 8577 (1995).
  - [44] E. Lindahl, B. Hess, and D. van der Spoel, *J. Mol. Model.* **7**, 306 (2001).
  - [45] H. J. C. Berendsen, J. P. M. Postma, W. F. van Gunsteren, A. Di-Nola, and J. R. Haak, *J. Chem. Phys.* **81**, 3684 (1984).
  - [46] B. Hess, H. Bekker, H. J. C. Berendsen, and J. G. E. M. Fraaije, *J. Comput. Chem.* **18**, 1463 (1997).
  - [47] W. Shinoda and S. Okazaki, *J. Chem. Phys.* **109**, 1517 (1998a).
  - [48] M. F. Brown, J. Seelig, and U. Häberlen, *J. Chem. Phys.* **70**, 5045 (1979).
  - [49] J.-P. Douliez, A. Léonard, and E. J. Dufourc, *Biophys. J.* **68**, 1727 (1995).
  - [50] H. I. Petrache, S. W. Dodd, and M. F. Brown, *Biophys. J.* **79**, 3172 (2000).
  - [51] K. V. Damodaran and J. K. M. Merz, *Biophys. J.* **66**, 1076 (1994).
  - [52] U. Essman, L. Perera, and M. L. Berkowitz, *Langmuir*. **11**, 4519 (1995).
  - [53] M. Hyvönen, T. T. Rantala, and M. Ala-Korpela, *Biophys. J.* **73**, 2907 (1997).
  - [54] W. Shinoda, M. Shimizu, and S. Okazaki, *J. Phys. Chem. B*. **102**, 6647 (1998b).
  - [55] A. M. Smondyrev and M. L. Berkowitz, *Biophys. J.* **77**, 2075 (1999).
  - [56] A. M. Smondyrev and M. L. Berkowitz, *Biophys. J.* **78**, 1672 (2000).
  - [57] R. F. Flewelling and W. L. Hubbel, *Biophys. J.* **49**, 541 (1986).
  - [58] S. A. Simon and T. J. McIntosh, *Proc. Natl. Acad. Sci. U.S.A.* **86**, 9263 (1989).
  - [59] K. Gawrisch, D. Ruston, J. Zimmerberg, V. A. Parsegian, R. P. Rand, and N. Fuller, *Biophys. J.* **61**, 1213 (1992).
  - [60] T. J. McIntosh, S. A. Simon, D. Needham, and C.-H. Huang, *Biochemistry*. **31**, 2020 (1992).
  - [61] P. H. Hünenberger and J. A. McCammon, *Biophys. Chem.* **78**, 69 (1999).
  - [62] W. Weber, P. H. Hünenberger, and J. A. McCammon, *J. Phys. Chem. B*. **104**, 3668 (2000).



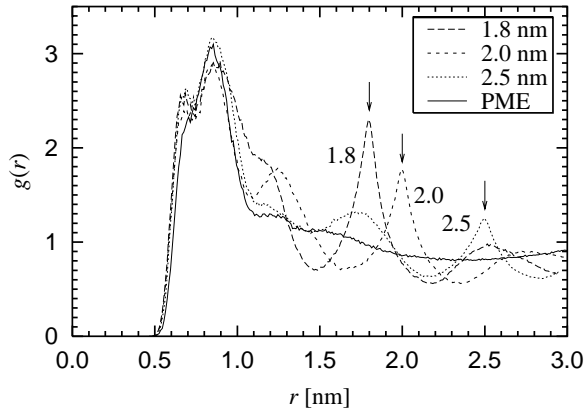


FIG. 10: Radial distribution function for N–N pairs in the head groups of DPPC molecules based on simulations with a van der Waals cutoff  $r_{\text{vdW}} = 1.4$  nm [cf. Fig. 8 with  $r_{\text{vdW}} = 1.0$  nm]. Cutoff distances are indicated by arrows.

#### APPENDIX A: EFFECT OF OTHER SIMULATION PARAMETERS

We have complemented the main body of research by further simulations to check the importance of other simulation parameters in the present work. For example, we have checked the importance of constraints by keeping the DPPC bonds flexible, investigated the role of pressure coupling by a study in which the time constant of the barostat was set to a

value of 5 ps, and repeated all the simulations at a temperature of  $T = 325$  K. In all cases we have found that both the quantitative results and the conclusions remain the same. However, changing the cutoff of the van der Waals interaction  $r_{\text{vdW}}$  appears to have effects worth noticing. While the parameterization of DPPC was done with a cutoff of  $r_{\text{vdW}} = 1.0$  nm, and was therefore used in the major part of this study, the value of 1.4 nm is also a common choice. This is motivated in particular by the Gromos96 forcefield which assumes  $r_{\text{vdW}} = 1.4$  nm.

Simulations similar to those with  $r_{\text{vdW}} = 1.0$  nm have been run with  $r_{\text{vdW}} = 1.4$  nm. The average area per lipid using PME is reduced by  $0.051 \text{ nm}^2$ , while the average areas per lipid for the three different cutoffs —  $r_{\text{cut}} = 1.8$  nm, or 2.0 nm, or 2.5 nm — are reduced by 0.017, 0.046, and  $0.067 \text{ nm}^2$ , respectively. This trend is understandable since an increase in  $r_{\text{vdW}}$  effectively increases the attractive interaction between acyl chains, thus reducing the area per molecule. Interestingly, also the average volume per lipid is reduced by about  $0.03 \text{ nm}^3$ , as was revealed by the Voronoi analysis of lipid bilayers in three dimensions. Despite these quantitative difference between the different cutoff distances for the van der Waals interactions, the conclusions of our work remain intact. This is demonstrated in Fig. 10, which presents data for the RDFs between the N–N pairs with a cutoff  $r_{\text{vdW}} = 1.4$  nm. The data indicate that the truncation of electrostatic interactions still gives rise to artificial ordering, which is not observed in the case of PME.